RSC Advances

PAPER

View Article Online
View Journal | View Issue

Cite this: *RSC Adv.*, 2021, **11**, 39467

Rice husk biochar modified-$CuCo_2O_4$ as an efficient peroxymonosulfate activator for non-radical degradation of organic pollutants from aqueous environment†

Kai Xie,[ab] Ruirui Han,[c] Ping Sun,[a] Hui Wang,[a] Yingsen Fang,*[a] Zhicai Zhai,[a] Danzhu Ma[b] and Hui Liu*[a]

Received 15th September 2021
Accepted 6th December 2021

DOI: 10.1039/d1ra06914d

rsc.li/rsc-advances

A series of rice husk biochar (RHBC) modified bimetallic oxides were prepared using a simple pyrolysis method to activate peroxymonosulfate (PMS) for the degradation of acid orange G (OG). The results demonstrated that 50 mg L^{-1} OG was completely decomposed by 1 mM PMS activated with 100 mg L^{-1} RHBC–$CuCo_2O_4$ within 15 min at initial pH 3.4. The OG degradation rate constant k of RHBC–$CuCo_2O_4$/PMS (0.95×10^{-1} min^{-1}) was five times greater than that of $CuCo_2O_4$/PMS (0.19×10^{-1} min^{-1}), suggesting that the introduction of RHBC significantly improved the activity of bimetallic oxides. The effects of the initial pH, catalyst dosage, PMS concentration and reaction temperature on OG removal were also studied. The degradation products of OG were analysed using a gas chromatography-mass spectrometer (GC-MS). Electron paramagnetic resonance (EPR) and quenching experiments showed that singlet oxygen ($^1O_2$) was the main active species. The RHBC–$CuCo_2O_4$/PMS oxidation system is not only unaffected by inorganic anions (Cl^-, NO_3^-, HCO_3^-) and humic acid (HA), but also could remove other typical pollutants of acetaminophen (ACT), sulfathiazole (STZ), rhodamine B (RhB), and bisphenol A (BPA). These findings show that RHBC–$CuCo_2O_4$ has great potential for practical applications in the removal of typical organic pollutants.

1. Introduction

In recent years, the problem of water pollution caused by rapid industrial development has become increasing significant and has attracted worldwide attention.[1,2] Recently, several works have considered the remediation of environmental water pollution. The Fenton method with hydroxyl radicals ($^{\bullet}OH$) as the main active material and the advanced oxidation of persulfate (AOPs) with sulfate radicals ($SO_4^{\bullet-}$) as the main active material have attracted much attention. After in-depth study, it is found that the traditional advanced oxidation method with $^{\bullet}OH$ as the main active substance cannot avoid some shortcomings of hydroxyl itself, such as short half-life (10^{-3} μs), narrow pH range (2–4) and that only part of the organic matter can be effectively degraded. The $SO_4^{\bullet-}$ based advanced oxidation technology has a higher redox potential (E_0 = 2.5–3.1 V) than that of $^{\bullet}OH$ (E_0 = 1.8–2.7 V), and $SO_4^{\bullet-}$ has a longer half-life (30–40 μs) than that of $^{\bullet}OH$. The advantages of wider pH applicable range and more stable effect with organic matter.[3–7] However, peroxymonosulfate (PMS) is a mild oxidant, and its degradation efficiency of organic pollutants is not significant at room temperature. Therefore, it needs to be activated under heat, UV exposure, ultrasound or transition bimetallic oxides to produce $SO_4^{\bullet-}$ with higher oxidation abilities, which then degrades the refractory organic compounds (POPs) in the environment.[8–12] Among the various studied methods, transition metal catalyst-activated PMS has been considered to be more feasible and effective. Among them, Co^{2+} is considered to be one of the best metal ions to activate PMS, but the environmental toxicity of dissolved Co limits its wide application.[13–15] Therefore, heterogeneous catalysts containing. Cobalt and its derivative complexes have been developed to activate PMS and avoid the potential leaching of metals. To date, $CuCo_2O_4$ bimetallic oxide with a spinel structure and general formula AB_2O_4 shows more potential in activating PMS because of its good chemical stability. Although these heterogeneous activation methods

[a]College of Biological, Chemical Sciences and Engineering, Jiaxing University, Jiaxing 314001, Zhejiang, PR China. E-mail: fangyingsen@zjxu.edu.cn; leolau@163.com
[b]College of Petroleum Engineering, Liaoning Petrochemical University, Fushun 113001, Liaoning, PR China
[c]College of Advanced Materials and Engineering, Jiaxing Nanhu University, Jiaxing 314001, Zhejiang, PR China

† Electronic supplementary information (ESI) available: XRD patterns of CuO, Co_2O_3, and recycle RHBC–$CuCo_2O_4$, N_2 sorption isotherms and pore size distributions of different materials (RHBC, $CuCo_2O_4$, RHBC–$CuCo_2O_4$), a possible pathway of OG oxidation degradation, the biodegradation efficiency of RHBC–$CuCo_2O_4$ for different pollutant, the surface porosity of various materials and degradation of pollutants by different catalysts. See DOI: 10.1039/d1ra06914d

overcome the disadvantage of leached metal ions form homogeneous systems into the environment, there is still the problem of low reaction rates.[16]

To enhance the activity and stability of the catalyst, the composite materials of metal oxides and carbon-based catalysts used to activate PMS has attracted increasing attention.[17–19] Carbon-based materials usually include activated carbon (AC),[18,20] carbon nanotubes (CNT),[21,22] graphene oxide (GO)[23–25] and biochar (BC).[26,27] Some research reports have considered metal oxides as supported on carbon-based materials as catalysts to activate PMS. For example, $CuCo_2O_4$ doped AC was used to degrade the 3BF dye pollutant. The reaction rate (k) of $CuCo_2O_4$–AC was 5.2 times greater than that of $CuCo_2O_4$ alone, and the removal efficiency was still as high as 96% after 5 cycles.[20] GO supported $CuCo_2O_4$ was used to degrade bisphenol A (BPA), which showed that the BPA degradation rate reached 100% in 5 min with k value for $CuCo_2O_4$–GO that was 35.5 times that of $CuCo_2O_4$ alone.[23] Some studies reported the degradation of trimethoprim (TMP) from the sol–gel synthesis of $CuFe_2O_4$–MWCNT. One study showed that the degradation rate of TMP reached 90% in 24 min.[21] Among all considered carbon-based materials, BC is widely used as a support or catalyst because of its high surface area, porous structure and rich functional groups which impact the surface, high cost-effectiveness and environmental friendliness.[28–30]

For a long time, $SO_4^{\cdot-}$ and $^{\cdot}OH$ has been considered as the main way of persulfate oxidation to remove pollutants. However, in recent years, some studies have found that non-radical pathways, such as $^1O_2$, play a dominant role in the activation of persulfate by carbon-based material. Compared with the radical oxidation pathway, the non-radical oxidation pathway is relatively stable and less disturbed by water matrix.[20,21,31] Therefore, the removal efficiency and mechanism of pollutants by RHBC–$CuCo_2O_4$ non-radical activated persulfate should be studied urgently.

An RHBC-modified $CuCo_2O_4$ was synthesized using a simple pyrolysis method as an activator of PMS to further improve its stability and catalytic activity. The OG is a typical azo dye and, has attracted much attention due to its toxicity, mutagenicity, carcinogenicity and refractory degradation.[32] Therefore, OG was selected as the target pollutant to evaluate the catalytic performance of RHBC–$CuCo_2O_4$ on PMS. X-ray diffraction (XRD), scanning electron microscopy (SEM) and high-resolution transmission electron microscopy (HRTEM) were used to characterize the morphology and composition of the RHBC–$CuCo_2O_4$ catalyst. The effects of the catalyst dosage, PMS concentration, initial pH value and reaction temperature on the RHBC–$CuCo_2O_4$/PMS oxidation system were studied. The mechanism for the RHBC–$CuCo_2O_4$/PMS oxidation system was discussed based on radical quenching experiments and EPR analysis.

2. Experimental section

2.1 Chemicals and materials

The RHBC was purchased from Qinfeng Zhongcheng Biomass New Materials Co., Ltd (Nanjing). The PMS was purchased from Aladdin Biochemical Technology Co., Ltd. The cobalt nitrate hexahydrate ($Co(NO_3)_2\cdot 6H_2O$), copper nitrate trihydrate ($Cu(NO_3)_2\cdot 3H_2O$), anhydrous ethanol (EtOH, AR), sodium chloride (NaCl), sodium nitrate ($NaNO_3$), sodium bicarbonate ($NaHCO_3$), L-histidine (L-His, 99%), *tert*-butanol (TBA, 99%), *p*-benzoquinone (*p*-BQ, 99%), humic acid (HA, 99%), OG (96%), acetaminophen (ACT, 99%), rhodamine b (RhB, 99%) sulfathiazole (STZ, 99%), BPA (99%), and other reagents were purchased from Macklin Biochemical Technology Co., Ltd; The water used in the experiment was obtained from a Milli-Q ultrapure water machine (Millipore, USA).

2.2 Catalyst preparation

The catalyst was prepared using a pyrolysis method, in which the molar ratio of $Co(NO_3)_2\cdot 6H_2O$ to $Cu(NO_3)_2\cdot 3H_2O$ was 2 : 1, and the mass ratio of metal oxides to BC was 1 : 1. The initial temperature of the calcining process was 50 °C. The temperature was then increased to 150 °C at a rate of 10 °C min^{-1}, and kept for 60 min, Next, the temperature was increased to 300 °C at a rate of 10 °C min^{-1}, and kept for 240 min. The RHBC–$CuCo_2O_4$ catalyst was then allowed to naturally cool to room temperature, the prepared material is denoted as RHBC–$CuCo_2O_4$. The RHBC–CuO and RHBC–Co_3O_4 catalysts were prepared similarly.

2.3 Characterization of catalysts

The FEI F20TWINJEM-2100F TEM (FEI, USA) and FEI NANO450 SEM (FEI, USA) were used for morphological analysis of the samples. The microstructure of the samples was characterized using an XR-7000 for X-ray diffraction (XRD). An ESCALAB250XI was used for X-ray photoelectron spectroscopy (XPS) (Thermo Fisher Scientific, USA) to quantitatively analyse the element content and morphology of the materials. The N_2 sorption data were obtained using an ASAP2020 specific surface area (SSA) and a porosity analyser (Micromeritics, USA).

2.4 Experiment procedures

The degradation experiments were performed in a water bath shaker at 25 °C. A total of 100 mL of 50 mg L^{-1} OG pollutant was added into a 250 mL conical flask, while the oxidant PMS and catalyst were subsequently added. The reaction system was sampled at a certain time and passed, through a 0.45 μm filter membrane. The analysis was performed after methanol quenching. The effects of different conditions (type and amount of catalyst, amount of PMS, reaction temperature, different ions and water quality) on the OG degradation were studied. In addition, experiments for catalyst recycling and free radical quenching were performed. In the experiments, the OG degradation can be described using pseudo-first order kinetics. As shown in the eqn (1) as below:

$$\ln\left(\frac{C_t}{C_0}\right) = -kt \quad (1)$$

where C_t is the OG concentration at time t, mM; C_0 is that initial OG concentration, mM; t is the reaction time, min; and k is the rate constant of the pseudo-first-order reaction, min^{-1}.

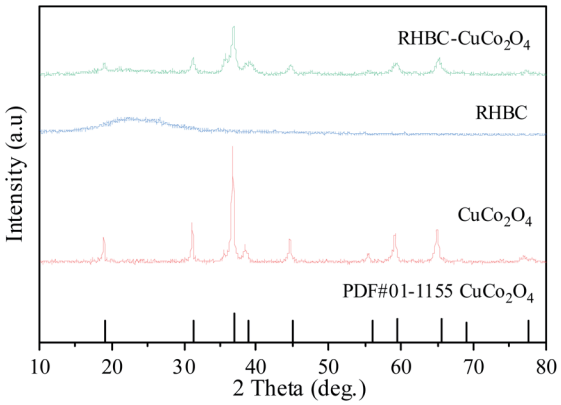

Fig. 1 XRD patterns of RHBC–$CuCo_2O_4$.

2.5 Analytical methods

The residual concentration of OG and RhB in the reaction system were detected using UV spectrophotometer, at detection wavelengths 475 nm and 554 nm, respectively. The residual concentrations of ACT, STZ and BPA were determined form high performance liquid chromatography (LC-20A, Shimadzu, Japan) with a photodiode array detector (SPDM20A). A Zorbax SB-C18 column (4.6 × 250 mm, 5 μm) (Agilent, USA) was used at a column temperature of 30 °C. A mixture of methanol (A)/0.3% formic acid solution (B) (30 : 70, v/v, for ACT and STZ; 70 : 30, v/v, for BPA) was used as the mobile phase at a flow rate of 1.0 mL min^{-1}. Total organic carbon (TOC) was determined using a TOC analyzer (Elementar, Germany). The degradation products were detected using a 7890B/5977C GC-MS (Agilent, USA). The reactive oxide species (ROS) generated form the system was detected using an EPR spectrometer (Bruker A320, USA).

3. Results and discussion

3.1 Characterization

The XRD characterization of the RHBC–$CuCo_2O_4$ is shown in Fig. 1. When preparing the RHBC–$CuCo_2O_4$, the RHBC characteristic peaks are not obvious due to its amorphous precursor. The 2θ peaks are 19.07°, 31.36°, 36.96°, 38.95°, 45.06° and 59.59°, which correspond to the characteristic peaks of $CuCo_2O_4$ (PDF # 01-1155).[33] This demonstrates the successful preparation of RHBC–$CuCo_2O_4$.

The morphologies of RHBC, $CuCo_2O_4$ and RHBC–$CuCo_2O_4$ were analysed *via* SEM and HRTEM, as shown in Fig. 2. In Fig. 2(A), the RHBC is an irregular blocky structure with a smooth surface, while Fig. 2(B) indicates the $CuCo_2O_4$ is composed of agglomerated nanoparticles.[33,34] When the $CuCo_2O_4$ is compounded with the RHBC, the nanoparticles of the $CuCo_2O_4$ are uniformly distributed on the surface of the RHBC (Fig. 2(C)), which indicates that the RHBC–$CuCo_2O_4$ was successfully synthesized. The RHBC, $CuCo_2O_4$, and RHBC–$CuCo_2O_4$ were further studied *via* HRTEM, as shown in Fig. 2(D), (E), and (F), respectively. The darker part in Fig. 2(D) is due to the multilayer bulk RHBC stack, the darker part in Fig. 2(E) is due to the opacity of the $CuCo_2O_4$ metal, and Fig. 2(F) shows the $CuCo_2O_4$ particles are uniformly distributed on the surface of the RHBC, which is consistent with the result of SEM images.[20,33]

The collected EDX spectrum is shown in Fig. 3(A), which indicates that the catalyst is composed of Co, Cu, C and O elements. Further elemental analysis shows that all elements were homogeneously distributed in the catalyst (Fig. 3(B–E)).[19,20,33] In addition, the pore volume and Brunner–Emmett–Teller (BET) obtained by measuring the adsorption/desorption of N_2 gave the specific surface area as shown in Fig. S2 and, Table S1.†

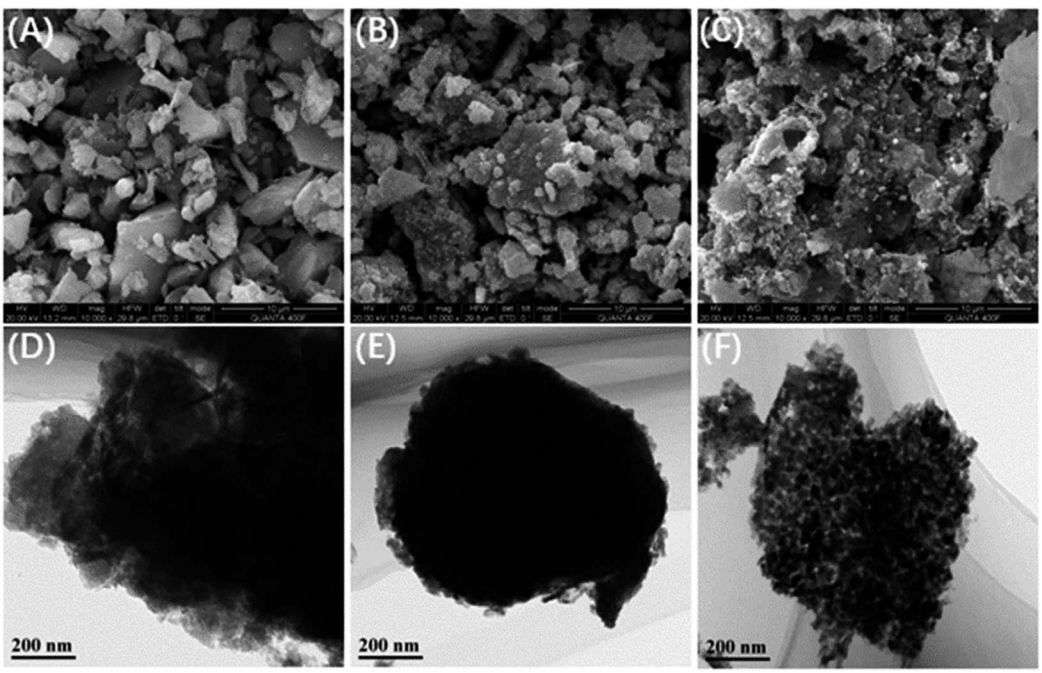

Fig. 2 SEM images of (A) RHBC, (B) $CuCo_2O_4$, and (C) RHBC–$CuCo_2O_4$; HRTEM images of (D) RHBC, (E) $CuCo_2O_4$, and (F) RHBC–$CuCo_2O_4$.

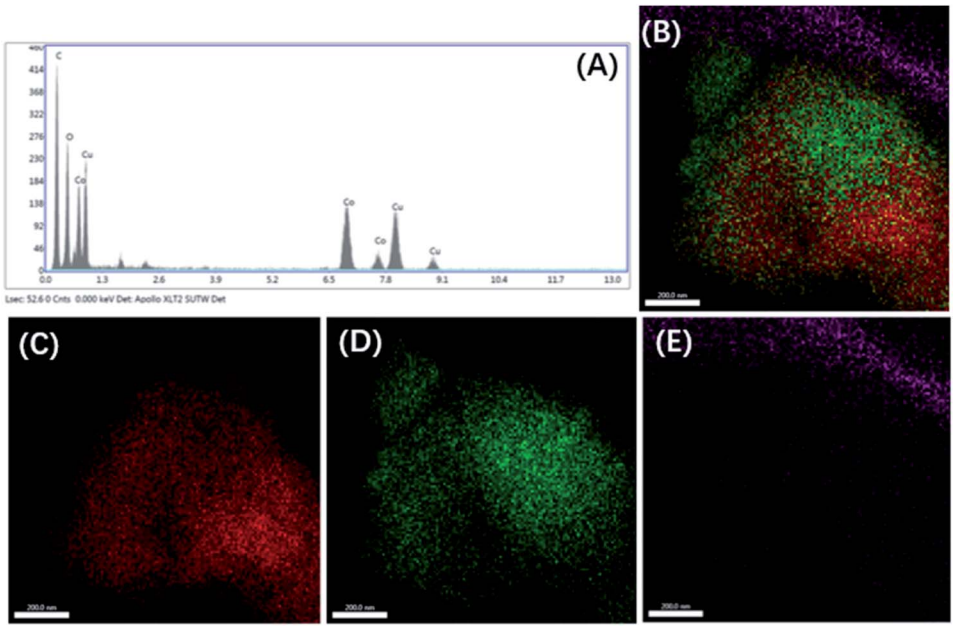

Fig. 3 (A) EDX spectrum, and elemental mapping images for (B) RHBC–$CuCo_2O_4$, (C) Co, (D) Cu, and (E) C.

3.2 Performance comparison of different catalyst

The catalytic performance of the RHBC–$CuCo_2O_4$/PMS system was evaluated using OG as the target contaminant, as shown in Fig. 4. The degradation of OG by PMS alone can be neglected as the removal efficiency was only 5% after 30 minutes of reaction. When the RHBC, CuO, Co_3O_4, $CuCo_2O_4$, RHBC–CuO, RHBC–Co_3O_4, and RHBC–$CuCo_2O_4$ were individually added to the PMS–OG mixed solution, the OG removal efficiency improved significantly. After reacting for 15 min, the PMS was activated by the RHBC–$CuCo_2O_4$, and the OG degraded completely. In contrast, the other catalysts showed incomplete degradations for OG within 30 min (*i.e.*, 6%, 27%, 17%, 60%, 97% and 80% OG removal by RHBC, CuO, Co_3O_4, $CuCo_2O_4$, RHBC–CuO and RHBC–Co_3O_4, respectively). These results show that the degradation performances of RHBC–CuO, RHBC–Co_3O_4, and RHBC–$CuCo_2O_4$ for OG are significantly improved compared with CuO, Co_3O_4, and $CuCo_2O_4$. The performance of RHBC–$CuCo_2O_4$ is improved by 40%, which indicates that the introduction of RHBC can enhance the catalyst activity to activate PMS and degrade OG.[18] To quantitatively determine the catalytic activity of the above kinetic curves, the pseudo-first-order reaction rate constants k were calculated as 0.13×10^{-2}, 0.89×10^{-2}, 0.51×10^{-2}, 0.19×10^{-1}, 0.32×10^{-1}, 0.25×10^{-1}, and 0.95×10^{-1} min^{-1}, indicating that RHBC–$CuCo_2O_4$ has an excellent catalytic activity to remove OG. Combined with the characterizations of Fig. 2 and Table S1,† this result may be due to the inhibition of $CuCo_2O_4$ agglomeration after loading RHBC, which results in a looser structure and a higher specific surface area (142.9 m^2 g^{-1}). This provides more active sites for more complete reactions, which is conducive to enhancing the catalytic activity of $CuCo_2O_4$.[20,23,24]

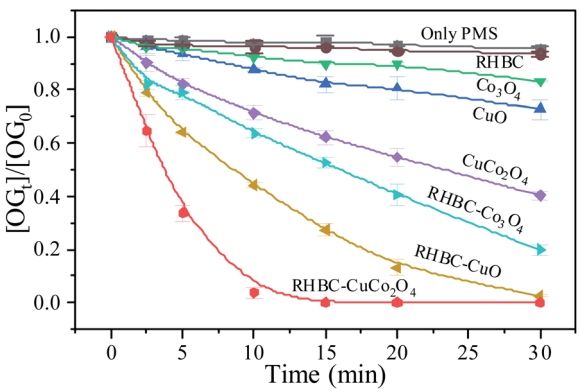

Fig. 4 Degradation efficiency of OG in different oxidation system. Condition: [OG] = 50 mg L^{-1}, [catalyst] = 100 mg L^{-1}, [PMS] = 307 mg L^{-1}, and T = 25 °C.

3.3 Influencing factors of catalytic oxidation process

The effect of the RHBC–$CuCo_2O_4$ dosage on OG degradation is shown in Fig. 5(A), The removal rate of OG increased significantly as the RHBC–$CuCo_2O_4$ dosage increased from 0 to 200 mg L^{-1}. When the mass concentration of RHBC–$CuCo_2O_4$ is 0 mg L^{-1}, PMS alone could not degrade the OG. When the mass concentration increased to 25 mg L^{-1}, the removal rate of OG was approximately 93% after 30 min of reaction. When the mass concentration increased to 50, 100, and 200 mg L^{-1}, the times of complete removal for OG were shortened to 30, 15, and 10 min, respectively. The k value of RHBC–$CuCo_2O_4$ were 0.32×10^{-2}, 0.48×10^{-1}, 0.95×10^{-1}, and 1.86×10^{-1} min^{-1} at concentrations of 25, 50 100, and 200 mg L^{-1}, respectively. This may be due to the increased amount of RHBC–$CuCo_2O_4$ catalyst, which provides additional active sites in the oxidation system and accelerates the production of ROS from the activated PMS.[20,35]

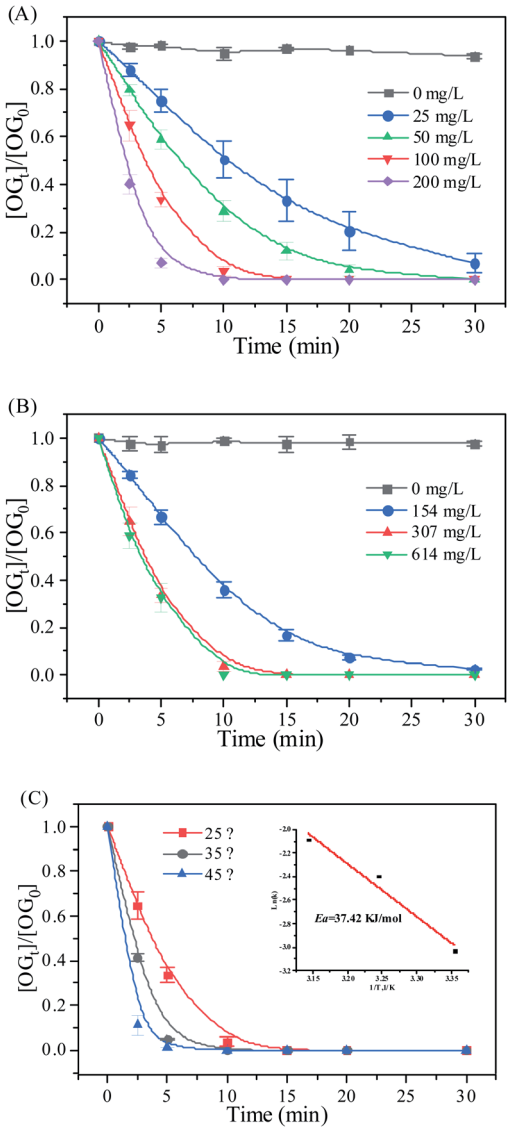

Fig. 5 (A) Dosage of RHBC–$CuCo_2O_4$, (B) dosage of PMS, and (C) effect of reaction temperature. Conditions: [OG] = 50 mg L^{-1}, [catalyst] = 0–200 mg L^{-1}, [PMS] = 0–614 mg L^{-1}, and T = 25–45 °C.

Fig. 5(B) illustrates the effect of the PMS dosage on OG removal. When the mass concentration of PMS was 154 mg L^{-1}, the OG could not be completely degraded. When the concentration of PMS was increased to 307 and 614 mg L^{-1}, the times for complete removal of OG were shortened to 15 and 10 min, and the k values increased from 3.39 × 10^{-2} min^{-1} to 0.95 × 10^{-1} and 1.35 × 10^{-1} min^{-1}, respectively. This is because when the PMS in the RHBC–$CuCo_2O_4$/PMS system is low, the generation rate of the ROS is limited. When the PMS dosage increases, the generation and rate of ROS increase, and the degradation rate of OG improves.[36]

Fig. 5(C) shows the effect of different temperatures the OG removal in the RHBC–$CuCo_2O_4$/PMS system. When the temperature increased from 25 to 45 °C, the effect of OG removal improved, because thermal activation is one of the important ways to activate persulfate, and increasing the temperature is generally conducive to the production of ROS by PMS.[8] At 25 °C, the degradation reaction was completed in 15 min. At 35 and 45 °C, the degradation reaction was shortened to 10 min. At 25, 35, and 45 °C, the k values of the oxidation system were 0.95 × 10^{-1}, 1.90 × 10^{-1}, and 1.98 × 10^{-1} min^{-1}, respectively. According to the Arrhenius equation, the calculated activation energy (E_a) of the oxidation system was 37.42 kJ mol^{-1}, indicating that the catalytic activity for RHBC–$CuCo_2O_4$ was less affected by the reaction temperature. Meanwhile, the E_a was lower than that of the $CuCo_2O_4$/PMS oxidation system as reported in the literature,[20,37] which has a better applicability and operability in practical applications.

3.4 Reaction mechanism analysis

To determine the ROS for OG degradation in the RHBC–$CuCo_2O_4$/PMS system, radical quenching experiments were performed by adding 0.5 M EtOH, 0.5 M TBA, 10 mM p-BQ, and 10 mM L-His as ROS quenchers to the solution. The EtOH can quench both $SO_4^{\cdot-}$ and $^{\cdot}OH$, TBA can quench $^{\cdot}OH$, p-BQ, and L-His can quench $O_2^{\cdot-}$ and $^1O_2$. As shown in Fig. 6(A), when p-BQ and L-His were added to the RHBC–$CuCo_2O_4$/PMS system, the removal rates of OG were only 65% and 42%, indicating that $O_2^{\cdot-}$ and $^1O_2$ may play major roles in OG degradation of. When EtOH and TBA were added, there was a slight effect on the OG degradation, indicating that $SO_4^{\cdot-}$ and $^{\cdot}OH$ may have minimal contributions.[32,35] The presence of significant ROS was further verified by EPR detection. As shown in Fig. 6(B) and (C), the signals for DMPO–OOH, DMPO–OH, DMPO–SO_4, and TEMP–$^1O_2$ were detected after PMS was activated by RHBC–$CuCo_2O_4$, which indicates the presence of $SO_4^{\cdot-}$, $^{\cdot}OH$, $O_2^{\cdot-}$, $^1O_2$ in the oxidation system.[38] Based on the results of the quenching experiments and EPR measurements, the sulphate, hydroxyl, superoxide, and singlet oxygen radicals coexist in the RHBC–$CuCo_2O_4$/PMS activation system. In addition, it is reported that $O_2^{\cdot-}$, as a precursor, participates as $^1O_2$, which may lead to $O_2^{\cdot-}$ playing an important role in OG degradation. It is also known that singlet oxygen radicals play a major role in OG degradation.[6,20,39,40]

The XPS spectra in Fig. 6(D–F), show the valence changes for Co and Cu and the oxygen content changes in the RHBC–$CuCo_2O_4$ catalyst before and after reactions to explore the activation mechanism of PMS. Five peaks (803.27, 795.39, 785.80, 780.87, and 779.46 eV) are shown in Fig. 6(D) for the XPS spectrum of Co 2p in RHBC–$CuCo_2O_4$ before the reaction.[17,41] Two obvious satellite peaks are located at 803.2 and 785.80 eV, respectively. 795.39 eV corresponds to the Co $2p_{1/2}$ peak, while Co(II) and Co(III) are located at 780.87 and 779.46 eV, respectively. The Co(II) content decreased from 64.8% to 54.5% and the Co(III) content increased from 35.2% to 45.5%, suggesting that both Co(II) and Co(III) may be involved in the PMS activation.[23,33,42] In Fig. 6(E), the XPS spectrum of Cu 2p in RHBC–$CuCo_2O_4$ before reaction shows four peaks (961.93, 953.83, 941.95, and 933.88 eV), in which two obvious satellite peaks are located at 961.93 and 941.95 eV. The Cu $2p_{1/2}$ peak position is at 953.83 eV, and Cu(II) is at 933.88 eV. After the reaction, Cu(I) increased from 0 to 50.98%, indicating that Cu(I) and Cu(II) may

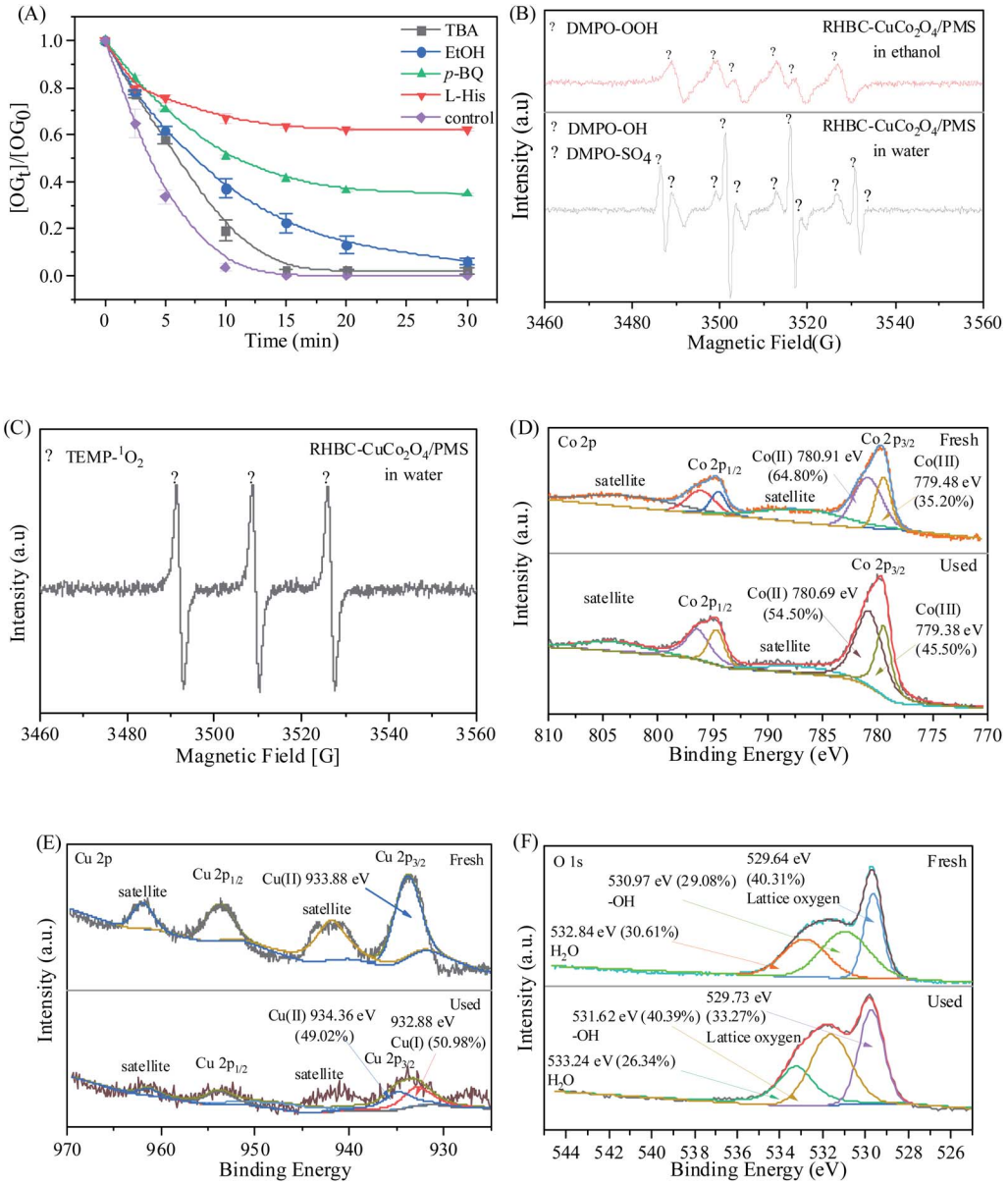

Fig. 6 Effect of different quenchers on the OG degradation by (A) RHBC–$CuCo_2O_4$/PMS; (B) DMPO–OOH, DMPO–OH, and DMPO–SO_4; (C) TEMP–$^1O_2$ complex; (D) Co 2p before and after the reaction; and XPS spectra of (E) Cu 2p and (F) O 1s. Conditions: [OG] = 50 mg L^{-1}, [catalyst] = 100 mg L^{-1}, [PMS] = 307 mg L^{-1}, T = 25 °C, [EtOH] = 0.5 M, [*p*-BQ] = [L-His] = 10 mM, and [DMPO] = [TEMP] = 50 mM.

also be involved in the PMS activation.[21,42,43] In Fig. 6(F), the –OH increased from 29.08% to 40.39% after the reaction, which may be due to the surface hydroxylation of RHBC–$CuCo_2O_4$.[33,44] Therefore, a possible OG degradation mechanism by the RHBC–$CuCo_2O_4$/PMS oxidation system is proposed. First, Co(III) and Cu(II) in the RHBC–$CuCo_2O_4$ are reduced by HSO_5^- to Co(II) and Cu(I) simultaneously to produce $SO_5^{\cdot-}$ (eqn (2)).[24,33,45] As $SO_5^{\cdot-}$ cannot directly degrade OG due to the low redox potential, it may contribute to the formation of $^1O_2$ (eqn (3) and (4)),[46] which is consistent with Fig. 6(F), as the lattice oxygen decreased from 40.31% before the reaction to 33.27% after the reaction. As $E^0_{Co(III)/Co(II)}$ (1.82 V) is higher than $E^0_{Cu(II)/Co(I)}$ (0.15 V), Co(III) and Cu(I) undergo electron transfer (eqn (5)), while Co(II) can react with H_2O to form surface hydroxylation, which is consistent with the increased –OH from 29.08% to 40.39% before the reaction in Fig. 6(F) (eqn (6)).[32,33] The O_2 generates $O_2^{\cdot-}$ through HSO_5^- transfer, before finally participating in the formation of $^1O_2$ (eqn (7) and (8));[20,33,47] The EPR results indicate a small amount of $SO_4^{\cdot-}$ and $^{\cdot}OH$ also participate in the reaction, eqn (9) and (10). Consequently, the OG is efficiently degraded by ROS, including $SO_4^{\cdot-}$, $^{\cdot}OH$, $O_2^{\cdot-}$, and $^1O_2$ to CO_2 and H_2O as described in eqn (11). Meanwhile, the removal rate of TOC can reach 7.8% after 30 min degradation in this reaction system, which may be due to the small dosage of oxidant PMS. When the dosage of PMS is increased by 5 times, the removal rate of TOC in this reaction system can reach 89.1%. Besides, the intermediates in

the degradation process of OG were analysed using an GC-MS, and the main intermediates were detected. It can be inferred that the degradation pathway of OG may be that $SO_4^{\cdot-}$, $^{\cdot}OH$, $O_2^{\cdot-}$ and $^1O_2$ first oxidizes the azo bond in the OG structure, making it decolorized and degraded into aromatic compounds with benzene ring and naphthalene nucleus as the main structure. Then the aromatic compounds are oxidized into oxygen-containing organic matter, and then decomposed into small molecular acid substances, and finally mineralized into CO_2 and H_2O (Fig S3†).

$$\equiv Cu(II)/\equiv Co(III) + HSO_5^- \rightarrow \equiv Cu(I)/\equiv Co(II) + H^+ + SO_5^{\cdot-} \quad (2)$$

$$2SO_5^{\cdot-} + H_2O \rightarrow 2HSO_4^- + 1.5\,^1O_2 \quad (3)$$

$$2\equiv Cu(I)/\equiv Co(II) + 2SO_5^- \rightarrow 2\equiv Cu(II)/\equiv Co(III) + 2SO_4^{2-} + {}^1O_2 \quad (4)$$

$$\equiv Cu(I) + \equiv Co(III) \rightarrow \equiv Cu(II) + \equiv Co(II) \quad (5)$$

$$\equiv Co(II) + H_2O \rightarrow \equiv Co(II) - OH^- + H^+ \quad (6)$$

$$3HSO_5^{\cdot-} + H_2O \rightarrow 3SO_4^{2-} + 2O_2^{\cdot-} + 5H^+ \quad (7)$$

$$O_2^{\cdot-} + e^- \rightarrow {}^1O_2 \quad (8)$$

$$\equiv Cu(I)/\equiv Co(II) + HSO_5^{\cdot-} \rightarrow \equiv Cu(II)/\equiv Co(III) + SO_4^{\cdot-} + OH^- \quad (9)$$

$$SO_4^{\cdot-} + OH^- \rightarrow {}^{\cdot}OH^- + SO_4^{2-} \quad (10)$$

$$SO_4^{\cdot-}/{}^{\cdot}OH^-/O_2^{\cdot-}/{}^1O_2 + OG \rightarrow \text{intermediates} \rightarrow CO_2 + H_2O \quad (11)$$

3.5 Environmental impact

Anions (Cl^-, NO_3^-, and HCO_3^-) and dissolved organic matter such as humic acid (HA) are widely present in real water bodies.[8,35] Therefore, inorganic anions and HA were added to the solution to simulate water bodies, and the effect of the oxidation system on the OG removal was investigated. As shown in Fig. 7(A), 5 mM of inorganic anions (HCO_3^-, Cl^-, NO_3^-) and 10 mg L^{-1} of HA showed no significant inhibitory effect on the RHBC–$CuCo_2O_4$/PMS system.

To further evaluate the effect of the RHBC–$CuCo_2O_4$/PMS oxidation system on removing pollutants in the actual water body, 50 mg L^{-1} of OG solution was prepared using both filtered tap water and river water, and a degradation experiment was used under the same experimental conditions described above. The experimental results shown in Fig. 7(A), indicate that the RHBC–$CuCo_2O_4$/PMS system can still effectively remove OG from tap and river waters.

Experiments were carried out at different pH values (3.4–9.0) to further study the catalytic performance of the RHBC–$CuCo_2O_4$/PMS system on the OG. Fig. 7(B) shows the OG

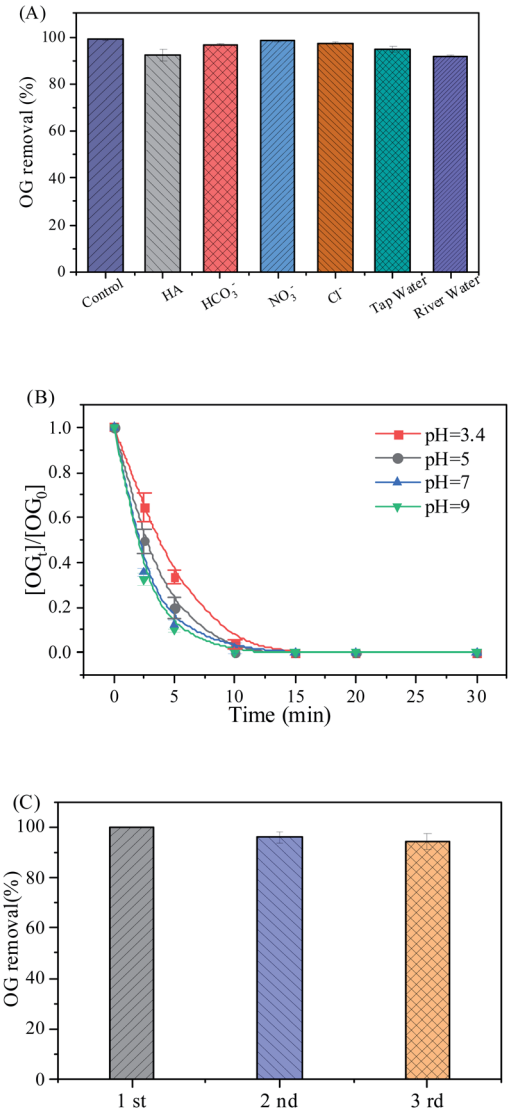

Fig. 7 (A) Effect of water on OG removal, (B) reaction pH value on OG removal efficiency, (C) stability of RHBC–$CuCo_2O_4$. Conditions: [OG] = 50 mg L^{-1}, [catalyst] = 100 mg L^{-1}, [PMS] = 307 mg L^{-1}, T = 25 °C, [Cl^-] = [NO_3^-] = [HCO_3^-] = 5 mM, and [HA] = 10 mg L^{-1}.

degradation form the RHBC–$CuCo_2O_4$/PMS system. The OG degradation rate was 100% and the k value was 0.95 × 10^{-1} min^{-1} at a pH of 3.4 and reaction time of 15 min. At pH values of 5, 7, and 9, the complete degradation time of OG was shortened to 10 min, and the k values were 0.16, 0.17, and 0.18 min^{-1}, respectively. The results showed that the degradation rate of OG increased with the pH. This may be due to the formation of interfacial repulsion between the PMS and the catalytic site (–OH) of the catalyst. This is caused by the connection of H^+ with negatively charged superoxide bonds (O–O) for the PMS at acidic pH values, which affects the degradation rate.[6,20] At a larger pH, the degradation rate increases, which may be due to two factors. On the one hand, more surface $^{\cdot}OH$ groups can enhance the electron density of transition metals and act as donor ligands to accelerate PMS activation.[48]

On the other hand, alkali treatment is a way to activate PMS, which accelerates the production of ROS.[49,50]

3.6 Reusability test of catalyst

The RHBC–$CuCo_2O_4$ was recovered from the aqueous solution *via* filtration after the reaction through a 0.45 μm organic membrane, washed three times with deionized water and ethanol, and then dried in a vacuum oven at 60 °C for 24 h. The stability of the RHBC–$CuCo_2O_4$ catalyst was then evaluated in the OG degradation experiment. Fig. 7(C) indicates that the OG degradation rate decreased slightly after 30 min of recycling, which decreased to 95% and 94% after the second and third uses, respectively. This may be due to the active sites being covered by the adsorbed organics, which results in the loss of active sites on the catalyst surface. Then, the catalytic performance for RHBC–$CuCo_2O_4$ was studied with four typical organic pollutants: ACT, STZ, BPA, and RhB. The reaction conditions were the same as the OG degradation process, and the degradation results are shown in Fig. S4.† After 30 min, the degradation rates of all pollutants reached 93–100%. Thus, RHBC–$CuCo_2O_4$/PMS, has the potential to degrade typical organic pollutants. In addition, RHBC–$CuCo_2O_4$ has a comparable catalytic performance with the other carbon–$CuCo_2O_4$ catalysts reported in the literatures (Table S2†).

4. Conclusion

The RHBC–$CuCo_2O_4$ prepared *via* pyrolysis has excellent performance when activating PMS to degrade OG. The results show that the OG degradation efficiency by RHBC–$CuCo_2O_4$/PMS was 40 times higher than that of $CuCo_2O_4$/PMS, which reached 100% in 15 min. In the RHBC–$CuCo_2O_4$/PMS system, anions (Cl^-, NO_3^-, and HCO_3^-) and HA did not affect the degradation reactions. Combined with the results of radical quenching experiments and EPR, the catalytic degradation process in RHBC–$CuCo_2O_4$/PMS followed a non-self-radical pathway, with singlet oxygen $^1O_2$ being the main active species. The results show that RHBC–$CuCo_2O_4$ has good stability and the OG degradation efficiency was still 94% after three cycles. In addition, the degradation rate of the RHBC–$CuCo_2O_4$ catalyst for the four typical pollutants (ACT, STZ, BPA and RhB) reached 93–100%, indicating that RHBC–$CuCo_2O_4$ has the potential to degrade typical organic pollutants. Therefore, RHBC–$CuCo_2O_4$ is a promising catalyst to activate PMS and degrade organic contaminants in aqueous solution.

Conflicts of interest

There are no conflicts to declare.

Acknowledgements

This study was supported by the Zhejiang Provincial Natural Science Foundation of China (No. LY21B070007 and LY21B070008), the National Natural Science Foundation of China (No. 21607058), and the Public Welfare Research Project of Jiaxing (No. 2021AD10008 and 2020AY10005).

References

1 Q. Wang and Z. Yang, *Environ. Pollut.*, 2016, **218**, 358–365.
2 J. X. Shi, W. P. Huang, H. J. Han and C. Y. Xu, *Renewable Sustainable Energy Rev.*, 2021, **143**, 20.
3 W. Y. Peng, Y. X. Dong, Y. Fu, L. L. Wang, Q. C. Li, Y. J. Liu, Q. Y. Fan and Z. H. Wang, *Chem. Eng. J.*, 2021, **421**, 127818.
4 L. H. Gao, Y. J. Cao, L. Wang and S. Li, *Front. Environ. Sci. Eng.*, 2022, **16**(6), 77.
5 M. D. G. Luna, R. P. Gumaling, E. G. Barte, R. R. M. Abarca, S. G. Segura and M. C. Lu, *J. Hazard. Mater.*, 2022, **421**, 126713.
6 C. Wang, J. Y. Zhao, C. M. Chen and P. Na, *Appl. Surf. Sci.*, 2021, **562**, 150134.
7 Y. B. Ding, X. R. Wang, L. B. Fu, X. Q. Peng, C. Pan, Q. H. Mao, C. J. Wang and J. C. Yan, *Sci. Total Environ.*, 2021, **765**, 142794.
8 Y. J. Sun, J. J. Zhao, B. T. Zhang, J. Li, Y. B. Shi and Y. Zhang, *Chem. Eng. J.*, 2019, **368**, 553–563.
9 P. Sun, H. Liu, Z. C. Zhai, X. S. Zhang, Y. S. Fang, J. Tan and J. Q. Wu, *Chem. Eng. J.*, 2019, **356**, 262–271.
10 L. X. Zhang, R. Zhang, W. N. Wang, S. Han and P. F. Xiao, *RSC Adv.*, 2021, **11**, 20580.
11 J. Ali, W. L. Lei, A. Shahzad, J. Ifthikar, G. G. Aregay, I. I. Shahib, Z. Elkhlifi, Z. L. Chen and Z. Q. Chen, *Water Res.*, 2020, **181**, 115862.
12 M. Noorisepehr, K. Ghadirinejad, B. Kakavandi, A. R. Esfahani and A. Asadi, *Chemosphere*, 2019, **232**, 140–151.
13 P. D. Hu and M. C. Long, *Appl. Catal., B*, 2016, **181**, 103–117.
14 Q. Gao, G. S. Wang, Y. R. Chen, B. Han, K. S. Xia and C. G. Zhou, *Environ. Sci.: Water Res. Technol.*, 2021, **7**, 1197–1211.
15 B. Bouzayani, E. Rosales, M. Pazos, S. C. Elaoud and M. A. Sanroman, *J. Cleaner Prod.*, 2019, **228**, 222–230.
16 A. R. Patel, G. Patel, G. Maity, S. P. Patel, S. Bhattacharya, A. Putta and S. Banerjee, *ACS Omega*, 2020, **5**, 30416–30424.
17 R. Tabit, O. Amadine, Y. Essamlali, K. Danoun, A. Rhihil and M. Zahouily, *RSC Adv.*, 2018, **8**, 1351.
18 L. Chen, S. Yang, X. Zuo, Y. Huang, T. M. Cai and D. H. Ding, *Chem. Eng. J.*, 2018, **354**, 856–865.
19 J. S. M. Nithya, J. Y. Do and M. Kang, *J. Ind. Eng. Chem.*, 2018, **57**, 405–415.
20 S. Chen, X. Liu, S. Y. Gao, Y. C. Chen, L. J. Rao and Z. W. Wu, *Environ. Res.*, 2020, **183**, 109245.
21 J. Kong, R. Li, F. L. Wang, P. Chen, H. J. Liu, G. G. Liu and W. Y. Lv, *RSC Adv.*, 2018, **8**, 24787–24795.
22 X. Chen, W. D. Oh and T. T. Lim, *Chem. Eng. J.*, 2018, **354**, 941–976.
23 X. Q. Xu, Y. B. Feng, Z. H. Chen, S. B. Wang, G. H. Wu, T. L. Huang, J. Ma and G. Wen, *Sep. Purif. Technol.*, 2020, **251**, 117351.
24 R. Noroozi, M. Gholami, M. Farzadkia and A. J. Jafari, *Int. J. Environ. Anal. Chem.*, 2020, 1718669.

25 F. J. Ren, W. W. Zhu, J. Y. Zhao, H. T. Liu, X. Zhang, H. Zhang, H. Zhu, Y. Peng and B. Wang, *Sep. Purif. Technol.*, 2020, **241**, 116690.
26 Y. You, Z. K. Shi, Y. H. Li, Z. J. Zhao, B. He and X. W. Cheng, *Sep. Purif. Technol.*, 2021, **272**, 118889.
27 P. T. Huong, K. Jitae, T. M. Al Tahtamouni, N. L. M. Tri, H. H. Kim, K. H. Cho and C. Lee, *J. Water Process. Eng.*, 2020, **33**, 101037.
28 S. Z. Wang and J. L. Wang, *Chemosphere*, 2020, **239**, 124812.
29 Q. R. Wang, Y. X. Shi, S. Y. Lv, Y. Liang and P. F. Xiao, *RSC Adv.*, 2021, **11**, 18525.
30 H. D. Xu, Y. C. Zhang, J. J. Li, Q. Q. Hao, X. Li and F. H. Liu, *Environ. Pollut.*, 2020, **257**, 113610.
31 L. Liu, Y. Li, Y. Pang, Y. Q. Lan and L. X. Zhou, *Chem. Eng. J.*, 2020, **401**, 126014.
32 X. Zhang, Y. Z. Qin, W. T. Zhang, Y. L. Zhang and G. H. Yuan, *Water Sci. Technol.*, 2020, **82**, 185–193.
33 C. Chen, L. Liu, Y. X. Li, W. Li, L. X. Zhou, Y. Q. Lan and Y. Li, *Chem. Eng. J.*, 2020, **384**, 123257.
34 B. Saravanakumar, G. Ravi, R. K. Guduru and R. Yuvakkumar, *J. Sol-Gel Sci. Technol.*, 2020, **94**, 241–250.
35 P. Sun, H. Liu, M. B. Feng, Z. C. Zhai, Y. S. Fang, X. S. Zhang and V. K. Sharma, *Appl. Catal., B*, 2020, **272**, 119005.
36 P. Sun, H. Liu, M. B. Feng, X. S. Zhang, Y. S. Fang, Z. C. Zhai and V. K. Sharma, *Sep. Purif. Technol.*, 2021, **268**, 118697.
37 Y. Feng, J. H. Liu, D. L. Wu, Z. Y. Zhou, Y. Deng, T. Zhang and K. M. Shih, *Chem. Eng. J.*, 2015, **280**, 514–524.
38 J. H. He, T. P. Xie, T. H. Luo, Q. Xu, F. Ye, J. B. An, J. Yang and J. K. Wang, *Ecotoxicol. Environ. Saf.*, 2021, **216**, 112189.
39 P. Sun, H. Liu, M. B. Feng, L. Guo, Z. C. Zhai, Y. S. Fang, X. S. Zhang and V. K. Sharma, *Appl. Catal., B*, 2019, **251**, 335–345.
40 Y. B. Zhou, Y. L. Zhang and X. M. Hu, *J. Colloid Interface Sci.*, 2020, **575**, 206–219.
41 Y. C. Hong, J. L. Peng, X. G. Zhao, Y. Yan, B. Lai and G. Yao, *Chem. Eng. J.*, 2019, **370**, 354–363.
42 C. Chen, L. Liu, J. Guo, L. X. Zhou and Y. Q. Lan, *Chem. Eng. J.*, 2019, **361**, 1304–1316.
43 H. P. Luo, B. Sheng, X. Y. Chen, Y. H. Wang, Q. Y. Chen and J. Zhou, *J. Hazard. Mater.*, 2021, **411**, 125050.
44 X. H. Fan, H. Lin, J. J. Zhao, Y. C. Mao, J. X. Zhang and H. Zhang, *Sep. Purif. Technol.*, 2021, **272**, 118909.
45 Y. P. Wang, H. D. Ji, W. Liu, T. S. Xue, C. Liu, Y. T. Zhang, L. Y. Liu, Q. Wang, F. Qi and B. B. Xu, *ACS Appl. Mater. Interfaces*, 2020, **12**, 20522–20535.
46 X. Y. Wang, W. T. Zhao, X. W. Wu, T. H. Zhang, Y. Liu, K. Zhang, Y. H. Xiao and L. L. Jiang, *Appl. Surf. Sci.*, 2017, **426**, 1198–1205.
47 Y. T. Peng, H. M. Tang, B. Yao, X. Gao, X. Yang and Y. Y. Zhou, *Chem. Eng. J.*, 2021, **414**, 128800.
48 S. Y. Zuo, D. S. Xia, Z. Y. Guan, F. Yang, J. Zan, H. M. Xiu, M. Z. Huang and D. Y. Li, *Colloids Surf., A*, 2021, **611**, 125895.
49 S. Y. Li, J. Huang, X. K. Li and L. S. Li, *Chem. Eng. J.*, 2020, **39**, 125529.
50 Y. Wang, Y. Wu, Y. F. Yu, T. Pan, D. T. Li, D. Lambropoulou and X. Yang, *Water Res.*, 2020, **186**, 116326.